JACS
JOURNAL OF THE AMERICAN CHEMICAL SOCIETY

COMMUNICATION

pubs.acs.org/JACS

Copper Nitride Nanocubes: Size-Controlled Synthesis and Application as Cathode Catalyst in Alkaline Fuel Cells

Haibin Wu and Wei Chen*

State Key Laboratory of Electroanalytical Chemistry, Changchun Institute of Applied Chemistry, Chinese Academy of Sciences, 5625 Renmin Street, Changchun 130022, China

Supporting Information

ABSTRACT: Copper nitride nanocubes are synthesized in a facile one-phase process. The crystal size could be tuned easily by using different primary amines as capping agents. Such Pt-free nanocrystals exhibit electrocatalytic activity toward oxygen reduction and appear to be promising cathodic electrocatalysts in alkaline fuel cells.

Size- and shape-controlled synthesis of metal and semiconductor nanocrystals has attracted much attention because most of their important physical and chemical properties, such as their catalytic and optical properties, are often size and shape dependent.[1−4] Due to the high electrocatalytic activity of Pt and Pd metals, most of the investigations for designing novel anode and cathode electrocatalysts for fuel cells have focused on nanostructured Pt- and Pd-based alloys.[5,6] However, due to the high cost and limited reserve of Pt and Pd, extensive research has also been devoted to the development of non-Pt materials as electrocatalysts for fuel cells.[7,8] In recent years, copper complexes have attracted enormous interest due to their significant electrocatalytic activities as both anodic and cathodic catalysts.[9−11] For example, Brushett et al.[9] reported that a carbon-supported copper complex of 3,5-diamino-1,2,4-triazole exhibited oxygen reduction catalytic performance comparable to that of a Pt/C cathode.

In recent years, metal[3,12] or metal alloy,[13,14] metal oxide,[15,16] and semiconductor[17−19] nanocubes have been successfully prepared by various synthetic methods. Nanocubes with specific exposed surfaces provide ideal model nanocrystals for the studies of surface-dependent properties. However, there are still no reports on the synthesis and properties of metal nitride nanocubes. Copper nitride (Cu_3N) is regarded as one of the most promising materials for optical storage devices,[20,21] high-speed integrated circuits,[22] and microscopic metal links.[23,24] Since the first report of polycrystalline Cu_3N by Juza and Hahn in 1939,[25] related work has focused on the synthesis of Cu_3N films by various techniques.[24,26,27] However, despite extensive research on Cu_3N films, studies focusing on the synthesis and electrocatalytic properties of shaped Cu_3N nanocrystals are still scarce. Herein, we report a simple and effective procedure to synthesize cubic copper(I) nitride nanocrystals. The crystal size can be tuned easily by using different primary amines as capping agents. The electrocatalytic activity of the Cu_3N nanocubes for the cathode reaction of fuel cells (oxygen reduction reaction, ORR) was also investigated. The results demonstrate that the as-prepared Cu_3N nanocubes are promising Pt-free electrocatalysts for alkaline fuel cell applications.

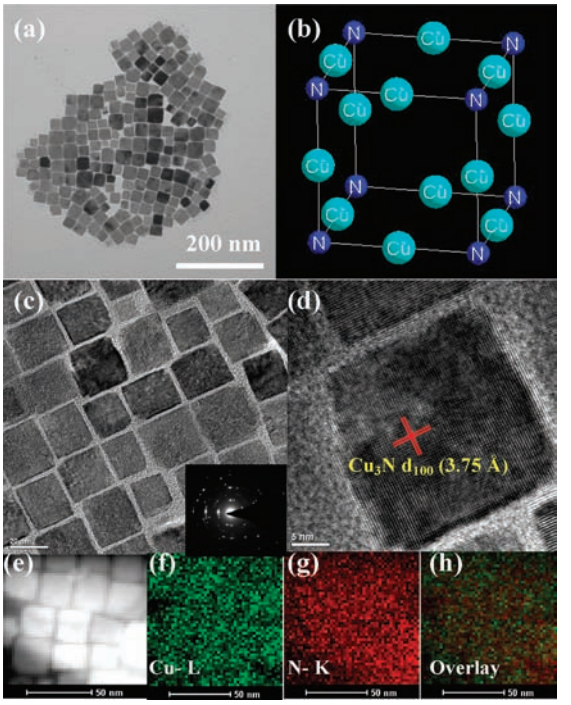

Figure 1. (a) Low-resolution TEM image and (b) the crystal structure of the Cu_3N nanocubes synthesized in a mixed solvent of octadecylamine and octadecene. (c,d) HRTEM images at different magnifications. The inset of (c) shows a SAED pattern of the nanocubes. (e) HAADF STEM image of the Cu_3N nanocubes, and the corresponding elemental mapping for (f) Cu, (g) N, and (h) the overlay.

Cubic Cu_3N nanocrystals were synthesized in organic solvents by a facile one-phase process. In a typical synthesis, copper(II) nitrate was dissolved in a mixed solvent of 1-octadecylamine and 1-octadecene. The reaction solution was heated at 150 °C for more than 3 h under magnetic stirring. During the reaction, the color of the solution changed from blue to green, and finally to yellow. The solution temperature was then raised to 250 °C at ~5 °C/min and kept for 30 min. The Cu_3N nanocubes were obtained by centrifugation and purification (see Supporting Information for details). Figure 1a shows a typical transmission electron microscopy (TEM) image of the Cu_3N nanocrystals, as synthesized in the mixed solution of octadecylamine and octadecene. The overall morphology of the nanocrystals is characterized

Received: May 24, 2011
Published: September 06, 2011

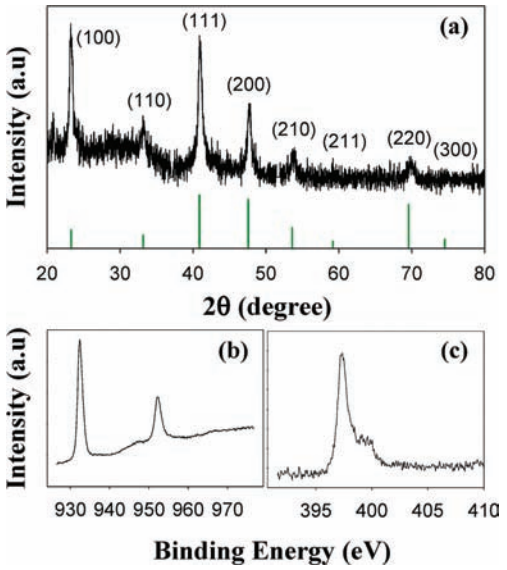

Figure 2. (a) XRD pattern of the Cu_3N nanocubes prepared in a mixed solvent of octadecylamine and octadecene. For comparison, bulk Cu_3N XRD data from the Joint Committee on Powder Diffraction Standard are also included (green bars). (b) Cu 2p and (c) N 1s XPS spectra.

by a uniform cubic shape with no impurity particles or aggregates. From the size histogram shown later in Figure 3b, the average size of the Cu_3N nanocubes was measured to be 26.0 ± 5.6 nm. From the UV/vis absorption spectrum (Figure S1), there is a broad absorption around 420 nm, corresponding to the electron−hole transition of the Cu_3N nanocrystals. Figure 1c,d displays high-resolution TEM (HRTEM) images at different magnifications, from which the highly crystalline nanocubes with well-resolved lattice fringes can be observed. Polycrystalline features were observed from the selected-area electron diffraction (SAED) pattern (Figure 1c, inset) because the SAED was recorded over multiple Cu_3N nanocrystals. Upon careful comparison with the HRTEM of a single Cu_3N nanocube (Figure 1d), the fringes with interplanar spacing of 3.75 Å can be indexed to the (100) plane of anti-ReO_3-structured Cu_3N with a lattice constant of 3.817 Å (JCPDS 47-1008; also see the crystal structure of Cu_3N shown in Figure 1b). To get further insight into the distribution of Cu and N in the as-synthesized Cu_3N nanocubes, elemental analysis was carried out with scanning transmission electron microscopy (STEM). Figure 1e shows a high-angle annular dark-field (HAADF) micrograph of a selected area of Cu_3N nanocubes. From the elemental maps of Cu and N and their overlay shown in Figure 1f−h, one can see that Cu and N are evenly distributed in the Cu_3N nanocubes. The energy-dispersive X-ray (EDX) spectrum shown in Figure S2 also indicates the presence of Cu and N in the sample. To the best of our knowledge, this is the first report of cubic Cu_3N nanocrystals synthesized by a wet chemical technique.

The crystal structure of the Cu_3N nanocubes was further examined with X-ray techniques. Figure 2a shows the powder XRD pattern of the as-prepared Cu_3N nanocrystals. The diffraction peaks could be indexed to the (100), (110), (111), (200), (210), (211), (220), and (300) planes of the Cu_3N. All the diffraction peaks agree well with the standard diffraction data for bulk Cu_3N, as shown as green bars in Figure 2a (from JCPDS No. 47-1088). No diffraction signal from impurities is present in the pattern, further indicating only a single Cu_3N phase in the product. It is worth noting that, in the XRD pattern from bulk Cu_3N, the intensity of the diffraction peak from (100) is much weaker than those of (111) and (200) planes. However, in the XRD pattern of the synthesized Cu_3N nanocubes, the diffraction peak from (100) is stronger than those from (111) and (200). This result suggests that abundant (100) planes exist in the present Cu_3N nanocrystals, in good agreement with the observation of (100) planes in the HRTEM measurements (Figure 1d). The oxidation states of Cu and N were also investigated with X-ray photoelectron spectroscopy (XPS). Figure 2b,c depicts the Cu 3p and N 1s XPS spectra of the sample. The strong peaks at ∼932.4 and 952.3 eV could be ascribed to the binding energies of the $2p^{3/2}$ and $2p^{1/2}$ electrons of Cu (I). Note that no peak from Cu (II) (∼940−950 eV) was observed. The sharp peak observed at 397.4 eV in the N XPS spectrum indicates the presence of nitrogen in the as-synthesized nanocubes. Both XRD and XPS measurements further verify the formation of Cu_3N nanocrystals by our synthetic protocol. The band gap of the synthesized Cu_3N nanocubes was also evaluated with electrochemical cyclic voltammetry (CV) measurements. On the basis of the onset redox potentials shown in Figure S3, the band gaps of the Cu_3N nanocubes are calculated to be 1.04 (indirect) and 1.5 eV (direct), which fall within the range of 1−1.9 eV reported previously.[24,26,28,29]

Primary amines are often used as protecting ligands for synthesizing metal or semiconductor nanomaterials. In the present study, 1-octadecylamine acts as both solvent and capping agent. It is well known that the preferential chemisorption of capping agents on particular facets could result in shape-controlled formation of nanocrystals. Here, preferential binding of 1-octadecylamine to the (100) facets of Cu_3N slows their growth rate, leading to the formation of cubic Cu_3N nanocrystals. The surface structure of the Cu_3N nanocubes was then examined by Fourier transform infrared (FTIR) measurements. Figure S4a,b shows the FTIR spectra of monomeric 1-octadecylamine and the Cu_3N nanocubes, respectively. Overall, the FTIR spectra from the as-synthesized Cu_3N nanocubes are quite similar to the spectrum of pure octadecylamine, except for the slight shifts of some peaks due to the interaction between capping agents and nanocrystals. The bands between 3250 and 3420 cm^{-1} are ascribed to the symmetric and antisymmetric vibration modes of −N−H. The $-NH_2$ scissoring mode and C−N stretching mode can be observed around 1578 and 1378 cm^{-1}, respectively. The bands within the range of 2800−3000 cm^{-1} are from the $-CH_2$ and $-CH_3$ symmetric and antisymmetric stretching vibrations. A sharp peak at ∼1464 cm^{-1} could be ascribed to the $-CH_2$ bending vibration. Such FTIR features suggest that 1-octadecylamine was indeed bound onto the nanocubes. However, an additional peak at ∼2092 cm^{-1} is also obvious in the FTIR spectrum of Cu_3N nanocubes. This absorption peak might be ascribed to the −C≡N stretching vibration mode, which was also observed in the previous FTIR measurements of oleylamine-stabilized silver nanoparticles.[30] The −C≡N group was probably transformed from the $-CH_2-NH_2$ during the high-temperature reaction.[30]

The effect of primary amines on the morphology and size of Cu_3N nanocrystals was further investigated. Figure 3 shows the TEM images and the corresponding size histograms of Cu_3N nanocrystals with different primary amines as capping agents. From the TEM image and size histogram shown in Figure 3a,b, it can be seen that Cu_3N nanocubes with an average size of 26.0 ± 5.6 nm were formed with 1-octadecylamine as protecting ligand.

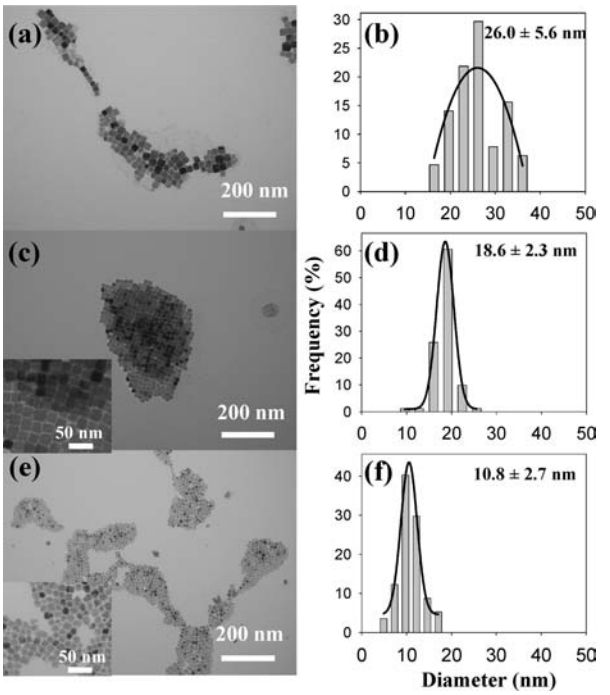

Figure 3. TEM images and the corresponding crystal size histograms of Cu_3N nanocrystals synthesized with different organic solvents: (a,b) octadecylamine and octadecene, (c,d) hexadecylamine and octadecene, and (e,f) oleylamine and octadecene. All the scale bars are 200 nm. The insets of (c) and (e) show magnified TEM images of the corresponding Cu_3N nanocubes.

With hexadecylamine instead of octadecylamine as capping agent, almost monodisperse Cu_3N nanocubes (Figure 3c) were obtained with an average size of 18.6 ± 2.3 nm (Figure 3d). Moreover, the Cu_3N nanocubes were self-assembled into a superlattice. When oleylamine was used as capping agent, cubic Cu_3N nanocrystals were also formed, as shown in Figure 3e; the observation of self-assembly of the nanocubes also suggests a uniform particle size. The mean diameter of the nanocrystals was further decreased to 10.8 ± 2.7 nm as shown in Figure 3f. These results demonstrate clearly that the crystal size of Cu_3N nanocubes can be controlled effectively by changing the amine capping agents. It should be noted that, in spite of the different particle sizes, the crystal structures of the Cu_3N nanocubes are similar, based on XRD, HRTEM, and other measurements (see Figure S5 for measurements of Cu_3N nanocubes obtained in oleylamine and octadecene). For instance, from the HRTEM image and XRD measurements (Figure S5b,c), the (100) plane is also abundant for the Cu_3N nanocubes capped with oleylamine. However, it was found that neither primary amines nor octadecene alone would produce Cu_3N nanocubes. For example, with the pure oleylamine as solvent and capping agent, it can be seen from the TEM image in Figure S6 that irregular Cu_3N nanocrystals with a wide size distribution were obtained. It should be pointed out that a ripening process is needed to obtain well-defined nanocubes. As shown in Figure S7, when the reaction solution was cooled suddenly from high temperature down to room temperature by injecting the hot solution quickly into methanol, only ill-defined nanocubes were obtained. Overall, the organic amine capping agents play important roles in the shape- and size-controlled synthesis of Cu_3N nanocrystals.

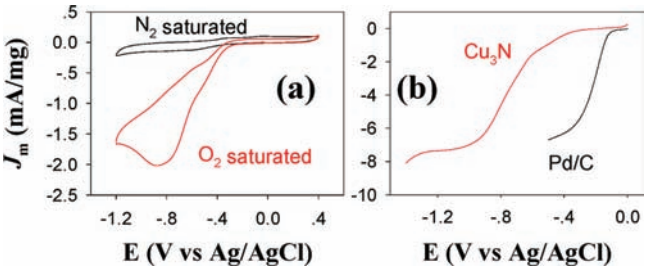

Figure 4. (a) CVs of Cu_3N nanocubes supported on glassy carbon substrate in N_2- or O_2-saturated 0.1 M KOH solution. Potential scan rate, 0.1 V s^{-1}. (b) Rotating disk voltammograms obtained on the Cu_3N nanocubes and Pd/C catalyst in 0.1 M KOH solution saturated with oxygen (3025 rpm; scan rate, 5 mV s^{-1}).

The electrocatalytic activity of the unsupported Cu_3N nanocubes was evaluated with electrochemical measurements by depositing 27.5 μg of the crystals on a glassy carbon electrode (referred to as Cu_3N/GC). Figure 4a shows the CVs of the Cu_3N nanocubes capped with octadecylamine in 0.1 M KOH saturated with either nitrogen or oxygen at a potential scan rate of 0.1 V s^{-1} (CVs with different potential scan rates are shown in Figure S8). Compared to the featureless CV profile in N_2-saturated electrolyte, a strong reduction current peak can be seen with the electrolyte saturated with O_2, suggesting the high electrocatalytic activity of the as-synthesized Cu_3N nanocubes toward oxygen cathodic reduction. ORR at Cu_3N/GC and commercial Pd/C catalyst with the same mass loading was also studied with rotating disk voltammetry (Figures S9 and S10). Figure 4b compares the rotating disk voltammograms of ORR at Cu_3N/GC and Pd/C catalysts. Despite the lower catalytic performance compared to that of traditional noble metal-based and some Pt-free catalysts,[31] the present Cu_3N nanocubes actually exhibit catalytic activity comparable with or even better than that of other non-Pt materials.[32] Such a novel non-Pt cathode electrocatalyst has potential applications in alkaline fuel cells, although more structural optimization is needed to further improve its catalytic performance. Ongoing work focuses on the shape-tuned synthesis of Cu_3N nanocrystals and detailed electrocatalytic investigations.

In summary, we have demonstrated a facile one-phase process to synthesize cubic Cu_3N nanocrystals. The crystal size was found to be tuned easily by using different primary amines as capping agents. This is the first time that metal nitride nanocubes have been synthesized. The as-synthesized Cu_3N nanocubes exhibit electrocatalytic activity toward oxygen reduction in electrochemical studies. Such Pt-free nanocrystals appear to be promising cathodic electrocatalysts in alkaline fuel cells. Large increases in catalytic activity are expected upon the further optimization of crystal structures.

■ ASSOCIATED CONTENT

Supporting Information. Detailed experimental procedures; additional structural characterizations and electrochemical measurements. This material is available free of charge via the Internet at http://pubs.acs.org.

■ AUTHOR INFORMATION

Corresponding Author
weichen@ciac.jl.cn

■ ACKNOWLEDGMENT

This work was supported by NSFC (No. 21043013) and startup funds for scientific research from Changchun Institute of Applied Chemistry, Chinese Academy of Sciences.

■ REFERENCES

(1) Mostafa, S.; Behafarid, F.; Croy, J. R.; Ono, L. K.; Li, L.; Yang, J. C.; Frenkel, A. I.; Cuenya, B. R. *J. Am. Chem. Soc.* **2010**, *132*, 15714–15719.
(2) Chen, W.; Chen, S. W. *Angew. Chem., Int. Ed.* **2009**, *48*, 4386–4389.
(3) Xia, Y.; Xiong, Y. J.; Lim, B.; Skrabalak, S. E. *Angew. Chem., Int. Ed.* **2009**, *48*, 60–103.
(4) Habas, S. E.; Lee, H.; Radmilovic, V.; Somorjai, G. A.; Yang, P. *Nat. Mater.* **2007**, *6*, 692–697.
(5) Chen, A. C.; Holt-Hindle, P. *Chem. Rev.* **2010**, *110*, 3767–3804.
(6) Bianchini, C.; Shen, P. K. *Chem. Rev.* **2009**, *109*, 4183–4206.
(7) Zhang, L.; Zhang, J. J.; Wilkinson, D. P.; Wang, H. J. *J. Power Sources* **2006**, *156*, 171–182.
(8) Morozan, A.; Jousselme, B.; Palacin, S. *Energy Environ. Sci.* **2011**, *4*, 1238–1254.
(9) Brushett, F. R.; Thorum, M. S.; Lioutas, N. S.; Naughton, M. S.; Tornow, C.; Jhong, H. R.; Gewirth, A. A.; Kenis, P. J. A. *J. Am. Chem. Soc.* **2010**, *132*, 12185–12187.
(10) Fukuzumi, S.; Kotani, H.; Lucas, H. R.; Doi, K.; Suenobu, T.; Peterson, R. L.; Karlin, K. D. *J. Am. Chem. Soc.* **2010**, *132*, 6874–6875.
(11) Patolsky, F.; Filanovsky, B. F., B.; Granot, E.; Dirawi, R.; Presman, I.; Kuras, I. *Nano Lett.* **2011**, *11*, 1727–1732.
(12) Sun, Y. G.; Xia, Y. N. *Science* **2002**, *298*, 2176–2179.
(13) Xu, D.; Liu, Z. P.; Yang, H. Z.; Liu, Q. S.; Zhang, J.; Fang, J. Y.; Zou, S. Z.; Sun, K. *Angew. Chem., Int. Ed.* **2009**, *48*, 4217–4221.
(14) Zhang, J.; Fang, J. Y. *J. Am. Chem. Soc.* **2009**, *131*, 18543–18547.
(15) Kim, D.; Lee, N.; Park, M.; Kim, B. H.; An, K.; Hyeon, T. *J. Am. Chem. Soc.* **2009**, *131*, 454–455.
(16) Park, J. C.; Kim, J.; Kwon, H.; Song, H. *Adv. Mater.* **2009**, *21*, 803–804.
(17) Zhang, J.; Kumbhar, A.; He, J. B.; Das, N. C.; Yang, K. K.; Wang, J. Q.; Wang, H.; Stokes, K. L.; Fang, J. Y. *J. Am. Chem. Soc.* **2008**, *130*, 15203–15209.
(18) Huxter, V. M.; Mirkovic, T.; Nair, P. S.; Scholes, G. D. *Adv. Mater.* **2008**, *20*, 2439–2440.
(19) Shen, H. B.; Wang, H. Z.; Chen, X.; Niu, J. Z.; Xu, W. W.; Li, X. M.; Jiang, X. D.; Du, Z. L.; Li, L. S. *Chem. Mater.* **2010**, *22*, 4756–4761.
(20) Asano, M.; Umeda, K.; Tasaki, A. *Jpn. J. Appl. Phys. Part 1* **1990**, *29*, 1985–1986.
(21) Maruyama, T.; Morishita, T. *Appl. Phys. Lett.* **1996**, *69*, 890–891.
(22) Borsa, D. M.; Grachev, S.; Presura, C.; Boerma, D. O. *Appl. Phys. Lett.* **2002**, *80*, 1823–1825.
(23) Maya, L. *J. Vac. Sci. Technol. A* **1993**, *11*, 604–608.
(24) Borsa, D. M.; Boerma, D. O. *Surf. Sci.* **2004**, *548*, 95–105.
(25) Juza, R.; Hahn, H. *Z. Anorg. Allg. Chem.* **1939**, *241*, 172–178.
(26) Kim, K. J.; Kim, J. H.; Kang, J. H. *J. Cryst. Growth* **2001**, *222*, 767–772.
(27) Pinkas, J.; Huffman, J. C.; Baxter, D. V.; Chisholm, M. H.; Caulton, K. G. *Chem. Mater.* **1995**, *7*, 1589–1596.
(28) Wang, D. Y.; Nakamine, N.; Hayashi, Y. *J. Vac. Sci. Technol. A* **1998**, *16*, 2084–2092.
(29) Du, Y.; Ji, A. L.; Ma, L. B.; Wang, Y. Q.; Cao, Z. *J. Cryst. Growth* **2005**, *280*, 490–494.
(30) Chen, M.; Feng, Y. G.; Wang, X.; Li, T. C.; Zhang, J. Y.; Qian, D. J. *Langmuir* **2007**, *23*, 5296–5304.
(31) Winther-Jensen, B.; Winther-Jensen, O.; Forsyth, M.; MacFarlane, D. R. *Science* **2008**, *321*, 671–674.
(32) Mentus, S. V. *Electrochim. Acta* **2004**, *50*, 27–32.